THE JOURNAL OF PHYSICAL CHEMISTRY B

Article

pubs.acs.org/JPCB

Replica-Exchange Molecular Dynamics Simulations of Cellulose Solvated in Water and in the Ionic Liquid 1-Butyl-3-Methylimidazolium Chloride

Barmak Mostofian,[†,‡] Xiaolin Cheng,[†,§] and Jeremy C. Smith*[,†,§]

[†]UT/ORNL Center for Molecular Biophysics, Oak Ridge National Laboratory, Oak Ridge, Tennessee 37830, United States

[‡]Graduate School of Genome Science and Technology, The University of Tennessee, Knoxville, Tennessee 37996, United States

[§]Department of Biochemistry, Cellular & Molecular Biology, The University of Tennessee, Knoxville, Tennessee 37996, United States

Supporting Information

ABSTRACT: Ionic liquids have become a popular solvent for cellulose pretreatment in biorefineries due to their efficiency in dissolution and their reusability. Understanding the interactions between cations, anions, and cellulose is key to the development of better solvents and the improvement of pretreatment conditions. While previous studies described the interactions between ionic liquids and cellulose fibers, shedding light on the initial stages of the cellulose dissolution process, we study the end state of that process by exploring the structure and dynamics of a single cellulose decamer solvated in 1-butyl-3-methyl-imidazolium chloride (BmimCl) and in water using replica-exchange molecular dynamics. In both solvents, global structural features of the cellulose chain are similar. However, analyses of local structural properties show that cellulose explores greater conformational variability in the ionic liquid than in water. For instance, in BmimCl the cellulose intramolecular hydrogen bond O3H′···O5 is disrupted more often resulting in greater flexibility of the solute. Our results indicate that the cellulose chain is more dynamic in BmimCl than in water, which may play a role in the favorable dissolution of cellulose in the ionic liquid. Calculation of the configurational entropy of the cellulose decamer confirms its higher conformational flexibility in BmimCl than in water at elevated temperatures.

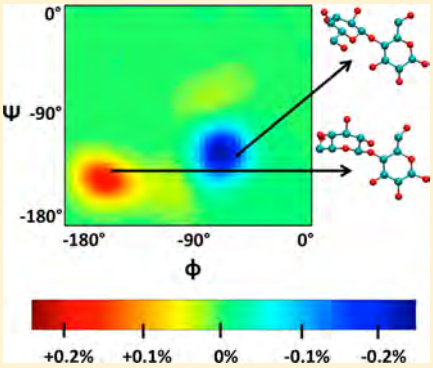

1. INTRODUCTION

Ionic liquids (ILs) are low melting point salts that are usually fluid below 100 °C. They often consist of an organic cation and a smaller anion. Because of their low volatility and reusability, ILs have been suggested to be of potential use in several industrial processes that involve chemical separation or synthesis.[1−6] One important field of application for ILs is the nonderivatized dissolution of lignocellulosic biomass before enzymatic hydrolysis.[7−11] In particular, the decomposition of cellulose, a glucose polymer that occurs in a fibrillar structure in plant cell walls, into smaller fermentable sugars has been shown to be more efficient after substrate pretreatment with imidazolium-based ILs.[12−17] Improved efficiency in biomass pretreatment is essential to the development of a sustainable biofuel industry based on renewable resources.[18−20] To this end, considerable research efforts have been focused on the search for ILs that facilitate cellulose dissolution,[21−24] as well as on understanding the molecular mechanisms that govern the dissolution process.[25−31]

Molecular dynamics (MD) simulations are useful in the analysis of interactions at atomic detail. Several MD studies have examined the effects of solvation of cellulose in water[32−34] or the free energy of single-chain detachment from microfibrils in aqueous solution.[35,36] Simulations of crystalline cellulose fibers in ILs such as 1-butyl-3-methylimidazolium chloride (BmimCl) or 1-ethyl-3-methylimidazolium acetate (EmimAc), which contain cations with an aromatic head and an aliphatic tail group, have revealed conformational changes of cellulose induced by the ionic solvent.[37,38] Recent studies have confirmed the hypothesis that anions, which usually have greater hydrogen bond basicity and thus make stronger hydrogen bonds with cellulose than water oxygens,[9] facilitate cellulose dissolution by breaking its intramolecular hydrogen bonds.[39] It has also been suggested that the less polar cation participates in the dissolution process, for example, through stacking and intercalation.[40−43] This finding seems plausible given the fact that cellulose is an amphiphilic molecule with exposed hydroxyl groups and hydrophobic pyranose rings. Hence, for efficient cellulose dissolution, both polar and nonpolar solvent components may be required[44,45] as provided by the most commonly used ILs.

The dissolution of cellulose by ILs involves the transition from the fiber state to the fully dissolved state of individual chains.[46] All-atom simulation of this entire process is not currently feasible due to the large system size (generally > 100 000 atoms) and the concomitant timescale limitation to the

Received: March 24, 2014
Revised: August 25, 2014
Published: September 2, 2014

dx.doi.org/10.1021/jp502889c | J. Phys. Chem. B 2014, 118, 11037−11049

sub-μs regime. Therefore, many previous studies have been focused on the simulation of a cellulose fiber solvated in water or in ILs, which sheds light on the initial stages of the dissolution process. Here, we study a single fully dissolved cellulose chain, which provides a description of the final state of dissolution. The comparative analysis of the thermodynamic and dynamic behavior of a cellulose chain fully solvated in water and in an IL can reveal differences in the effects of these two solvents, leading to a better understanding of the differential dissolution process and its driving forces.

Previously, short simulations (<5 ns) of single cellulose chains in EmimAc identified more favorable interactions between cellulose and the IL than between cellulose and other solvents.[40] Moreover, later simulations of solvent-penetrated cellulose chains in BmimCl have shown that the $Bmim^+$ and the Cl^- ions interact with distinct moieties of glucan residues.[47] However, because many conformational properties are known to take considerable time to converge in ILs, drawing major conclusions on the differences in solvation based on short simulations remains problematic due to limited sampling.

In this study, we use replica-exchange molecular dynamics (REMD) simulations to investigate the structure and dynamics of a cellulose decamer solvated in BmimCl and in water. REMD simulations have been widely used for the study of conformational equilibria in biomolecules.[48−51] With this method, noninteracting replicas of the molecular system are simulated simultaneously at different temperatures. Exchange of neighboring replicas at regular intervals reduces trapping in local minima and improves phase space sampling. Thus, through comparison of results on the two different solvent systems, differences in cellulose solvation mechanisms between the two solutions are found. The simulations cover a temperature range from 350 to beyond 500 K, which covers typical cellulose pretreatment temperatures, in water at ~375 K and in BmimCl at 425−450 K. The results reveal that, although global structural features of cellulose show no major differences between the BmimCl and water solutions, local conformational properties of cellulose differ significantly between the two solvents. These effects possibly result in their different dissolution abilities. The solute is more flexible and the solute−solvent interactions are more favorable in BmimCl than in water, particularly at elevated temperatures. Estimation of the intramolecular entropy contribution to the solvation free energy suggests that the configurational entropy of the cellulose chain may play a role in the more favorable solvation in ILs.

2. METHODS

A cellulose decamer (Figure 1a) was solvated in a cubic box with 1 330 BmimCl ion pairs (Figure 1b) and in a dodecahedral box with ~11 500 water molecules. Both systems comprised ~35 000 atoms. The GLYCAM06 molecular mechanics force field parameters[52] were used for the cellulose, and the TIP3P water model[53] was employed. BmimCl parameters had been developed previously,[54] and partial charges were assigned through fitting to electrostatic potentials computed at the Hartree−Fock level with the 6-31G* basis set using the GAUSSIAN program (see Supporting Information, Table S1).[55]

The solvated cellulose systems were first equilibrated at 350 K for 100 ps in the NVT ensemble and at the corresponding REMD target temperatures for 300 ps in the NPT ensemble. In all equilibration and REMD simulations, the temperature was

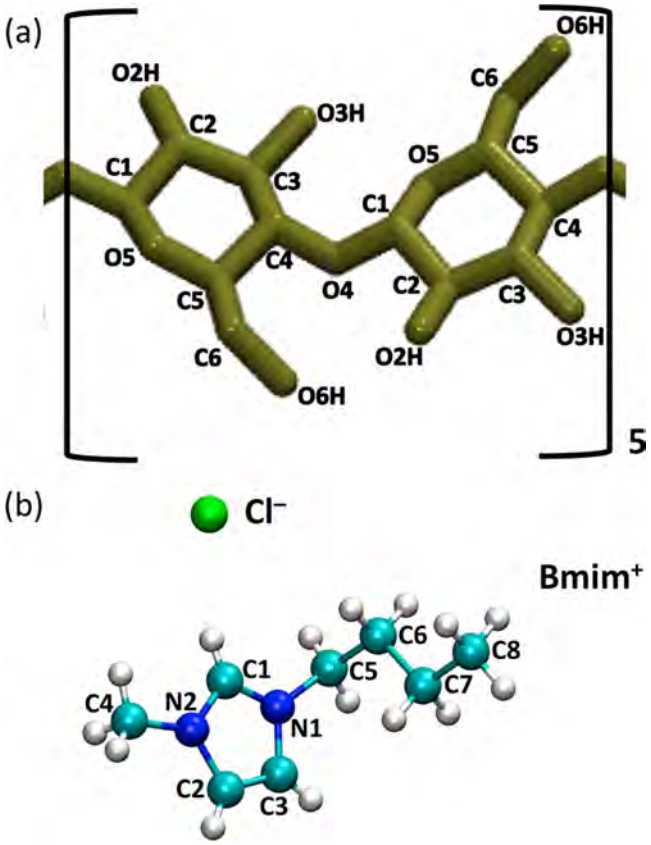

Figure 1. (a) Structure of the cellulose repeat unit. (b) Structure of BmimCl. The cation consists of an imidazole-containing head group and a butyl tail group.

maintained by velocity rescaling with a stochastic term to ensure proper sampling[56] and the pressure was controlled with the Berendsen barostat[57] with a coupling constant of 1 ps and an isothermal compressibility of 4.2×10^{-5} bar^{-1} for simulations in the IL[58] and 4.5×10^{-5} bar^{-1} for simulations in water. Periodic boundary conditions were applied and long-range electrostatic interactions were calculated using the particle-mesh Ewald summation[59,60] with a real-space cutoff at 12 Å. van der Waals interactions were cut off at 10 Å. The LINCS algorithm was used to fix the bond lengths containing hydrogens.[61] The simulation time step was 2 fs and coordinates were saved at every ps. All simulations were performed and analyzed with GROMACS.[62]

REMD simulations were performed in the NPT ensemble with a pressure correction term in the exchange probability.[63] Sixty replicas of the cellulose−BmimCl system covering a temperature range from 350 to 550 K were subjected to REMD, while 68 replicas of the cellulose−water system covered a temperature range from 350 to 513 K. For both systems, exchange probabilities were 15−18% averaged over 100 ns of REMD. The results in this paper are reported for a total simulation time of ~13 μs. More details on the REMD simulations are provided in the Supporting Information.

The cellulose configurational entropy was calculated using the quasi-harmonic method.[64,65] This approach estimates the absolute intramolecular entropy, S, based on a multivariate harmonic approximation of the configurational probability distribution:

$$S = \frac{1}{2}Nk_B + \frac{1}{2}k_B[\ln(2\pi)^N + \ln(|\mathbf{C}|)] \quad (1)$$

Here, N is the number of degrees of freedom, k_B is the Boltzmann constant, and $\mathbf{C}$ is the covariance matrix of the (internal) coordinates q, i.e., $\mathbf{C} = \langle(q - \langle q\rangle)\otimes(q - \langle q\rangle)\rangle$, where angular brackets indicate canonical ensemble averaging and $\mathbf{a}\otimes\mathbf{b}$ is the matrix with components ij equal to a_ib_i. According to Di Nola et al.,[66] the entropy consists of an uncorrelated diagonal part, S_{diag}, and an expression for the correlation correction, S_{corr}:

$$S_{diag} = \frac{1}{2}Nk_B + \frac{1}{2}k_B\left[\ln(2\pi)^N + \sum_i \ln(C_{ii})\right] \quad (2)$$

$$S_{corr} = \frac{1}{2}k_B \ln\left(\frac{|\mathbf{C}|}{\prod_i C_{ii}}\right) \quad (3)$$

Instead of applying the quasi-harmonic approximation, the diagonal part can be replaced with the exact entropy evaluation for every degree of freedom i, which gives

$$S = -k_B \sum_i \int dq_i P(q_i) \ln(P(q_i)) + \frac{1}{2}k_B \ln\left(\frac{|\mathbf{C}|}{\prod_i C_{ii}}\right) \quad (4)$$

We evaluate the configurational entropy in torsional space, which results in 120 degrees of freedom for the entire cellulose decamer. In these and all other profiles, mean values were computed as block averages over the simulation time and error bars (if given) correspond to one standard deviation.

3. RESULTS AND DISCUSSION

3.1. Cellulose Conformational Changes. The REMD enhanced-sampling method allows more rapid convergence of the dynamics of the simulated systems and greater exploration of conformational variation than standard MD. Efficient exchange of replicas and proper REMD performance are demonstrated by the potential energy distribution overlaps in Figure S1 and the exchange time series in Figure S2 of the Supporting Information. In the following, we analyze thermodynamic properties at temperatures relevant to the cellulose pretreatment process (e.g., T = 375 K in water or T = 450 K in BmimCl) and also examine the temperature dependence of these properties.

Through the enhanced sampling, a large number of cellulose structures were explored in both BmimCl and water. A basic parameter that quantifies the corresponding overall size of a polymer is the radius of gyration, R_g. In Figure 2, all sampled cellulose structures are characterized by R_g calculated using the glycosidic bond oxygens (O4):

$$R_g = \sqrt{\frac{1}{N_g}\sum_i^{N_g}(r_i(O4) - r_{mean}(O4))^2} \quad (5)$$

where $r_{mean}(O4)$ is the average position of the oxygen atom and N_g = 9 is the number of glycosidic bonds.

The sampled cellulose conformations range from elongated decamer structures to collapsed configurations (see Supporting Information, Figure S3). Temperature profiles based on R_g (Figure 2a) or on the cellulose end-to-end distance d (Supporting Information, Figure S3) both indicate that in both solvents the overall size of the decamer reduces with

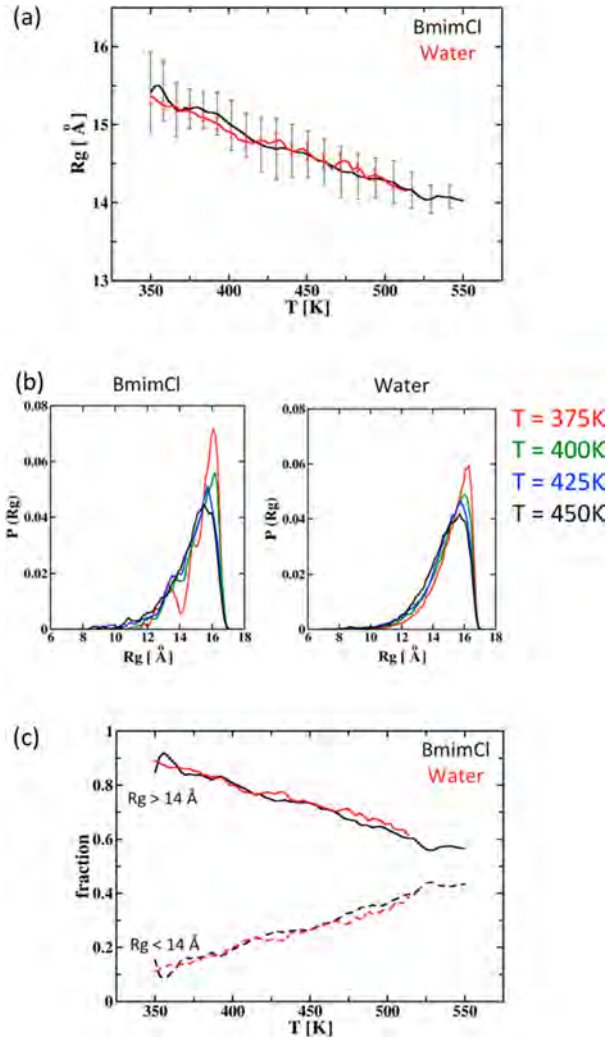

Figure 2. (a) Temperature profile of the radius of gyration, R_g, calculated using the cellulose linker oxygens O4 in BmimCl (black) and in water (red). (b) Distribution of R_g, $P(R_g)$, for cellulose structures in BmimCl (left) and in water (right) binned with ΔR_g = 0.1 Å at the four temperatures T = 375, 400, 425, and 450 K. Colors correspond to the given temperatures (see far right). In both solvents about three-quarters of all structures are extended with R_g > 14 Å. (c) Fraction of extended (R_g > 14 Å, solid lines) and compact (R_g < 14 Å, dashed lines) structures for cellulose in BmimCl (black) and in water (red).

increasing temperature. The polysaccharide does not collapse to a compact structure with increasing temperature but rather gradually reduces its stiffness and thus samples more conformations of smaller overall size at higher T. This behavior is qualitatively different from that in proteins that denature and expand upon increasing temperature and fold into a compact native state structure at lower, physiological temperatures. Negligible changes in the solvent-accessible surface area and in the solvent-excluded volume of cellulose (Supporting Information, Figure S4) both confirm that a sharp transition from an extended to a compact conformation does not occur.

The fact that the decrease of R_g or d as a function of the temperature is comparable in both solvents means that this temperature-dependent conformational change is not driven by specific interactions of the solute with water molecules or with BmimCl ions. However, in BmimCl both profiles show greater variation at any temperature as indicated by the larger error

dx.doi.org/10.1021/jp502889c | J. Phys. Chem. B 2014, 118, 11037−11049

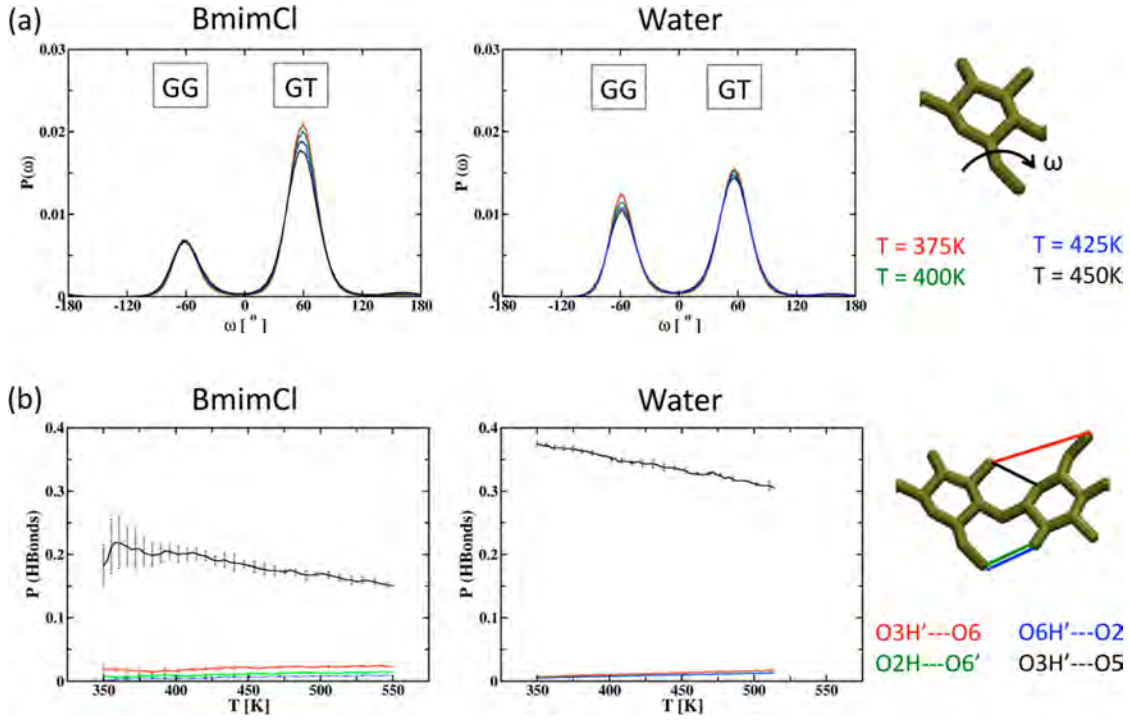

Figure 3. (a) Probability distributions of the cellulose hydroxymethyl angle ω (displayed on the far right) in BmimCl (left) and in water (right) for the four temperatures T = 375, 400, 425, and 450 K. The two preferred conformations around $\omega = -60°$ and $\omega = 60°$ are referred to as GG and GT, respectively. Colors correspond to the given temperatures (see far right). (b) Temperature profiles of occupancies for cellulose intramolecular hydrogen bonds O3H′···O6, O2H···O6′, O6H′···O2, and O3H′···O5 (displayed on the far right) between any two neighboring glucose units in BmimCl (left) and in water (right). Only the O3H′···O5 hydrogen bond is formed to a significant degree. Colors correspond to the given bonds (see far right).

bars, suggesting higher flexibility of cellulose in the IL than in water. On the basis of the value of R_g, any given cellulose decamer structure can be broadly classified as compact (R_g < 14 Å) or extended (R_g > 14 Å). According to this classification, in both solvents at any temperature the majority of all sampled cellulose structures is extended (Figure 2b). Interestingly, while ∼90% of cellulose structures are extended at the lowest simulation temperature, only ∼55% are extended at the highest temperatures (Figure 2c). This shows that the REMD approach broadly explores conformational space, sampling both compact and extended cellulose conformations at any temperature.

The cellulose decamer behaves like a semirigid rod polymer at lower temperatures, which is characteristic at length scales below a polymer's persistence length, L_P.[67] The values of L_P of cellulose in aqueous solution at room temperature reported in the literature are between ∼100 and ∼160 Å, significantly longer than the contour length of the decamer studied here.[68−70] By extrapolation, in the present REMD simulations L_P for the decamer is indeed estimated to be >10 glucose units at T < 400 K but decreases to 5 glucose units (∼26 Å) at T = 500 K in both solvents (Supporting Information, Figure S5). This explains why the cellulose decamer is mainly extended at lower temperatures and collapsed at higher temperatures in this study. The polymer structure of cellulose in the simulations is characterized and discussed in more detail in the Supporting Information.

Except for the greater flexibility of the solute in BmimCl, the present results on overall structural parameters such as the radius of gyration and the persistence length do not reveal a significant difference between the two solvents. However, in addition to these parameters, we investigated the rotamer conformations of the hydroxymethyl groups and the glycosidic bonds as well as the ability to form intramolecular hydrogen bonds or to maintain the six-membered ring of its glucose units in the favorable chair conformation (pyranose ring puckering).

The hydroxymethyl group of a glucose unit can adopt stable staggered rotamers, referred to as GG, GT, and TG, corresponding to the trans and gauche conformations of the O5−C5−C6−O6 and C4−C5−C6−O6 torsions. We define the angle ω as the former torsion. The distributions of ω at distinct temperatures for simulations in BmimCl and in water are given in Figure 3a. The TG conformation is populated at <1%. The GG and GT populations differ significantly between the BmimCl and water solutions. On average, ω adopts the GG conformation in ∼50% of cellulose configurations in water at the lowest temperature (T = 350 K) and in ∼40% at the highest temperature ($T \approx$ 513 K). Accordingly, the population values for the GT conformation range from ∼50% to ∼60% of cellulose structures with increasing simulation temperature in water. In BmimCl, however, the corresponding values for the GG and GT populations change from around 30% and 70% (at T = 350 K) to around 20% and 80% (T = 550 K), respectively, depending on the temperature. This result is similar to that found in previous simulations of cellulose oligomers of different lengths solvated in water or the IL 1-ethyl-3-methylimidazolium acetate (EmimAc).[40] Together, these results suggest that the preference of the GT over the GG conformation of the hydroxymethyl groups is higher in cellulose-dissolving ILs, such as EmimAc or BmimCl, than in water. Thus, the ratio P(GG)/P(GT) may serve as a parameter that distinguishes between the different structures the cellulose chain can adopt in the two solvents. The temperature dependence of this ratio is visualized

dx.doi.org/10.1021/jp502889c | J. Phys. Chem. B 2014, 118, 11037−11049

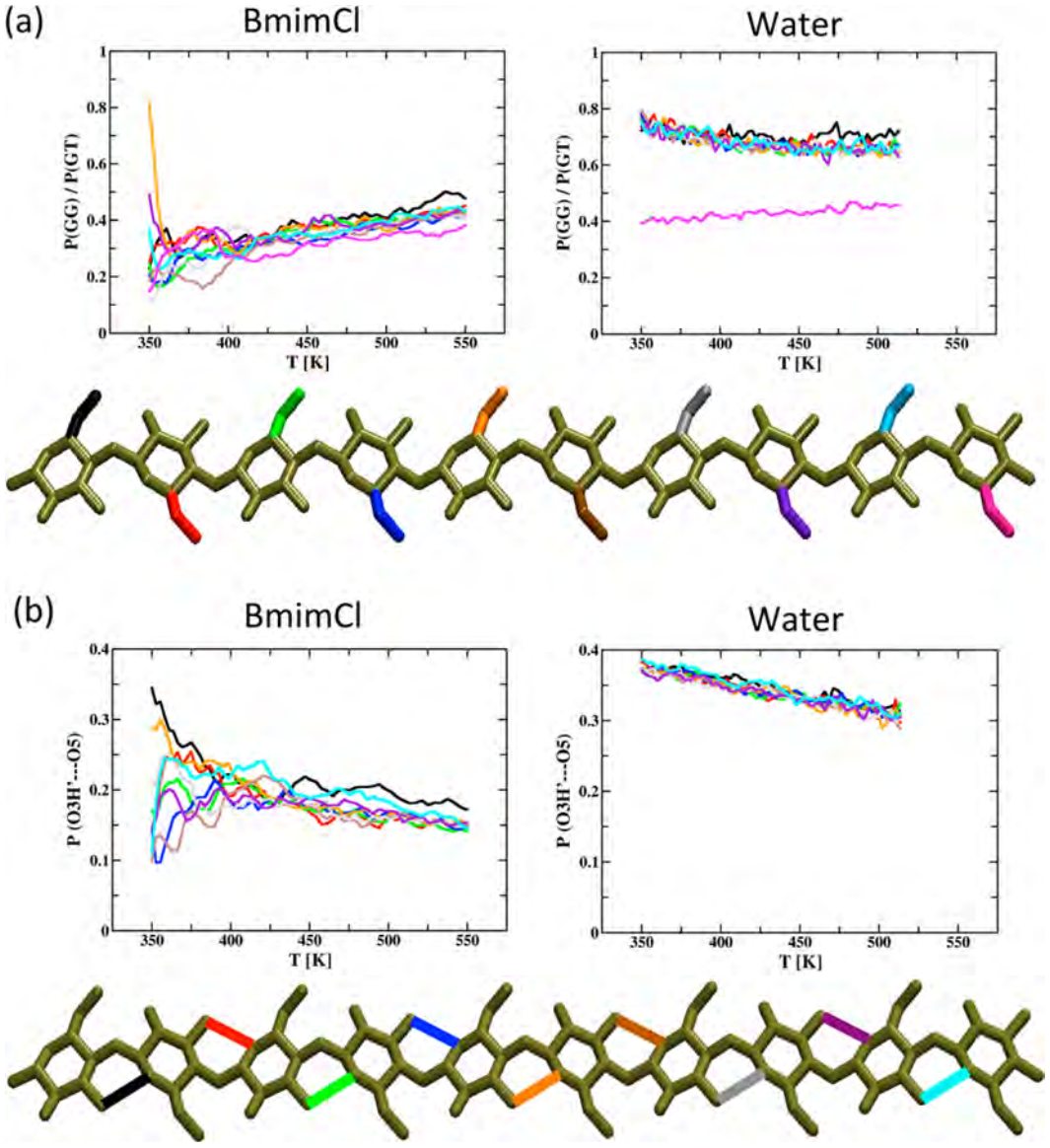

Figure 4. Temperature profiles for (a) the ratio of ω populations $P(\mathrm{GG})/P(\mathrm{GT})$ and (b) the intramolecular O3H′···O5 hydrogen bond occupancies $P(\mathrm{O3H'\cdots O5})$. Colors correspond to the hydroxymethyl group or hydrogen bond given below the corresponding graph.

as an average per glucose monomer in Figure 4a. $P(\mathrm{GG})/P(\mathrm{GT})$ is higher for cellulose in water (0.7−0.8) than in BmimCl (0.2−0.5). In the cellulose−water simulations, the value of $P(\mathrm{GG})/P(\mathrm{GT})$ decreases slightly with increasing T for all the hydroxymethyl groups except for the terminal group at the nonreducing end, which lacks a neighboring monomer. In contrast, in the cellulose−BmimCl simulations $P(\mathrm{GG})/P(\mathrm{GT})$ generally increases with T. It is worth noting that the corresponding distributions of this ratio also follow the same trends if we consider only compact (R_g < 14 Å) or extended (R_g > 14 Å) cellulose chains (data not shown).

In the Iα and Iβ forms of crystalline cellulose, intramolecular hydrogen bonds exist between O3H′···O5, O3H′···O6, O2H···O6′, and O6H′···O2 of neighboring monomers (where the prime labels the residue toward the reducing end).[71] In this study, we consider a hydrogen bond formed when the donor−acceptor distance is <3.5 Å and the hydrogen-donor−acceptor angle is <60°. The average occupancies of these hydrogen bonds as a function of simulation temperature are given in Figure 3b. The only hydrogen bond that is formed to any significant degree is O3H′···O5; all other hydrogen bond occupancies are <1%. With increasing temperature, the average O3H′···O5 occupancy, $P(\mathrm{O3H'\cdots O5})$, decreases from around 20% to 15% in BmimCl, while in water this value decreases from around 38% to 30%. Temperature profiles for individual O3H′···O5 hydrogen bond occupancies along the cellulose chain are shown in Figure 4b. With the exception of the cellulose−BmimCl simulations at low temperatures (350−400 K), $P(\mathrm{O3H'\cdots O5})$ assumes similar values for individual hydrogen bonds at any given temperature in either solvent.

These above results reveal clear differences between cellulose chains in BmimCl and in water in terms of the hydroxymethyl rotamer conformation and intramolecular hydrogen bonding. However, these two properties may be coupled to each other, as the hydroxymethyl conformation of a glucose residue could depend on the hydrogen bond state of its O5 atom. Thus, it is desirable to know how the conformational state of a hydroxymethyl rotamer changes with the adjacent O3H′···O5 hydrogen bond state. To this end, we analyzed the values of the hydroxymethyl angle, ω, as a function of the neighboring

dx.doi.org/10.1021/jp502889c | J. Phys. Chem. B 2014, 118, 11037−11049

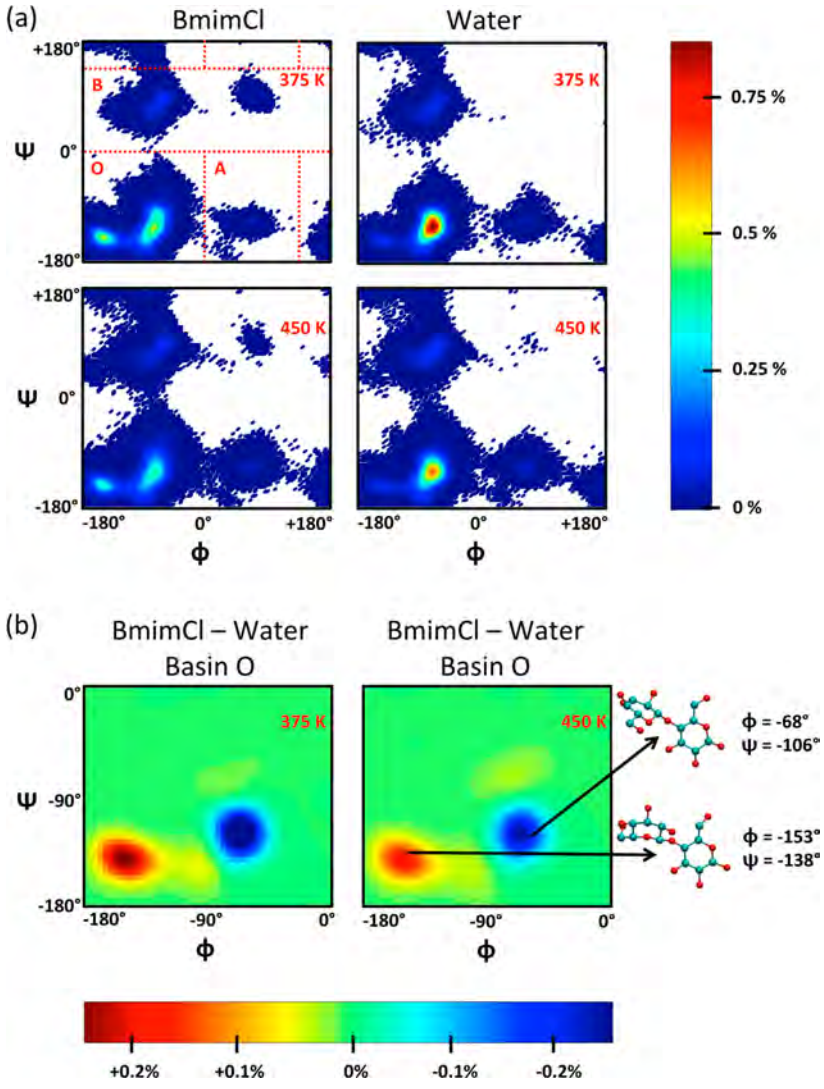

Figure 5. (a) Two-dimensional scatter plots for the glycosidic bond torsions ϕ and ψ binned with $(\Delta\phi, \Delta\psi) = (1°, 1°)$ for simulations in BmimCl and in water at the two temperatures 375 and 450 K. The three different basins O, A, and B are indicated in the top left scatter plot. (b) ϕ–ψ difference maps (BmimCl - Water) for the most populated basin O ($-180° < \phi/\psi < 0°$) at both temperatures. Two example cellobiose structures characterize the difference between structures from the "BmimCl basin" (red) and those from the "water basin" (blue).

O3H′···O5 hydrogen bond state in both solvents. We find that, in >75% of all cases in which the O3H′ hydrogen atom is bound to a solvent water oxygen or Cl^- anion and not to the O5 atom of the neighboring residue, the adjacent hydroxymethyl group assumes the GT conformation. This indicates that the intramolecular O3H′···O5 hydrogen bond is coupled to the hydroxymethyl conformation. In fact, the difference in ω populations between the two solvents, with ω assuming the GT conformation more frequently in BmimCl than in water, as discussed earlier, may be indirectly controlled by the greater hydrogen-bond basicity of Cl^- anions than water oxygens.

In Supporting Information, Figure S7, we visualize the correlation of the above two parameters, $P(GG)/P(GT)$ and $P(O3H'\cdots O5)$, in two-dimensional free energy landscapes based on population histograms for simulations at the corresponding cellulose pretreatment temperatures, i.e., at T = 375 K in water and at T = 450 K in BmimCl. For these and all following free energy landscapes, it should be mentioned that a value of 0.1% corresponds to >100 structures and that the standard deviation in the free energy basins is 0.01–0.02%. The most populated region of the free energy landscape in Supporting Information, Figure S7, is split into two basins along the ratio $P(GG)/P(GT)$. The two basins in the BmimCl simulations ($IL_{1/2}$) contain 23%–28% (depending on the simulation temperature) of the sampled cellulose structures while only ∼15% fall in the basins of the corresponding water simulations ($W_{1/2}$). However, the two energy basins cannot be distinguished from each other based on global features of the cellulose structures they contain. For instance, both extended and compact structures are found in either basin, and individual structures have comparable average potential energies and average solute–solvent interaction energies. Hence, cellulose structures with similar global properties can differ in local structural properties such as the order parameters $P(GG)/P(GT)$ and $P(O3H'\cdots O5)$, with the latter possibly leading to their different dissolution abilities.

The two torsional angles around the cellulose glycosidic bond, ϕ for C4′–O4′–C1–O5 and ψ for C5′–C4′–O4′–C1, define the backbone structure of the polysaccharide. Two-dimensional scatter plots of ϕ and ψ reveal three distinct regions of stable conformations, which have previously been referred to as basins O, A, and B (see Figure 5a).[70] The

dx.doi.org/10.1021/jp502889c | J. Phys. Chem. B 2014, 118, 11037–11049

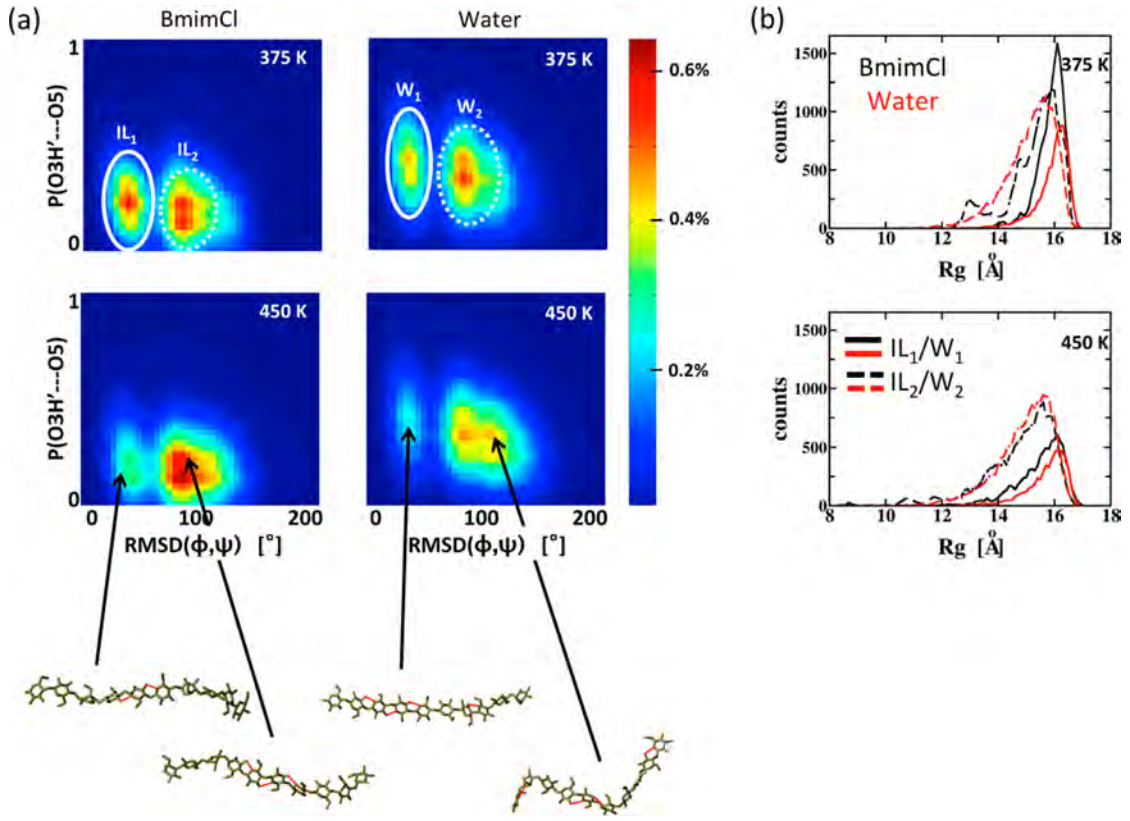

Figure 6. (a) Free energy landscape for the order parameters RMSD(ϕ,ψ) and P(O3H′···O5) for simulations in BmimCl (left) and in water (right) at T = 375 (top) and T = 450 K (bottom). The two distinct basins in each plot are referred to as $IL_{1/2}$ and $W_{1/2}$. Representative structures for each basin are given on the bottom (O3H′···O5 hydrogen bonds are indicated in red). (b) Total count of cellulose structures in BmimCl (black) and in water (red) binned with ΔR_g = 1 Å for the four basins IL_1 (solid black), IL_2 (dashed black), W_1 (solid red), and W_2 (dashed red) at T = 375 (top) and T = 450 K (bottom).

populations of these different basins are similar for any individual glycosidic bond of the cellulose decamer: >80% can be attributed to basin O, <20% can be attributed to basin B, and a negligible amount can be attributed to basin A.

Comparison of ϕ−ψ plots reveals differences of populations in basins O and B between cellulose in BmimCl and in water (Figure 5a). For example, a small population occurs in basin B of the BmimCl simulations but not in that of the water simulations at $\phi \approx 90°$ and $\psi \approx 120°$. This additional ϕ−ψ conformation is mainly assumed by glycosidic bonds at the cellulose chain ends, which are more flexible in BmimCl than in water. In basin O, difference plots at T = 375 and at T = 450 K, respectively, highlight two distinct subregions that are preferably populated in water ("water basin", blue) or in BmimCl ("BmimCl basin", red). Representative structures from these two areas of the ϕ−ψ plot are also illustrated in Figure 5b. Regardless of the simulation temperature and solvent environment, the average O3H′···O5 separation is 4.2 Å for any cellobiose unit that falls in the BmimCl basin but only 2.5 Å for those in the water basin. The corresponding average hydrogen bond occupancies are <1% in the BmimCl basin but around 40% in the water basin, once more showing the destructive effect of the IL on the intramolecular O3H′···O5 hydrogen bond. This result indicates a correlation between this hydrogen bond and the backbone conformation. A similar population difference in basin O of the ϕ−ψ plot between water and IL solvated cellulose oligomers has been reported previously.[40] The authors found three distinct basins in basin O based on much shorter MD simulations (<5 ns).

The glycosidic bond torsions ϕ and ψ describe the orientation of two neighboring glucose units and so can be referred to as internal coordinates for the cellulose backbone. Hence, the root-mean-square deviation (RMSD) in ϕ−ψ space is a metric sensitive to structural changes of the cellulose. We define chain-averaged ϕ−ψ RMSDs as

$$\mathrm{RMSD}(\phi, \psi) = \sqrt{\frac{1}{N_g}\sum_{i=1}^{N_g} (\phi_i(t) - \phi_i(t_0))^2 + (\psi_i(t) - \psi_i(t_0))^2} \quad (6)$$

where the reference structure at t_0 is the REMD starting structure after the initial NVT equilibration with $\phi_i(t_0) = -83°$ and $\psi_i(t_0) = -32°$ for any glycosidic bond i and N_g = 9 is the number of glycosidic bonds.

Figure 6a shows free energy landscapes using RMSD(ϕ,ψ) and P(O3H′···O5) as the order parameters for T = 375 and T = 450 K. In all landscapes, there is a clear separation between a basin RMSD(ϕ,ψ) ≈ 45° (IL_1 or W_1) and another at RMSD(ϕ,ψ) ≈ 90° (IL_2 or W_2). Extended cellulose decamers (R_g > 14 Å) populate the basins IL_1/W_1 for the most part, while compact structures (R_g < 14 Å) generally fall into IL_2/W_2, as the distribution of basin-specific R_g values indicates (Figure 6b). Thus, consistent with our results on the temperature dependence of cellulose chain length (see Figure 2), the basins IL_1/W_1 depopulate with increasing temperature as more compact structures are sampled. Therefore, the chain-averaged RMSD of ϕ−ψ is shown to be a suitable parameter for

dx.doi.org/10.1021/jp502889c | J. Phys. Chem. B 2014, 118, 11037−11049

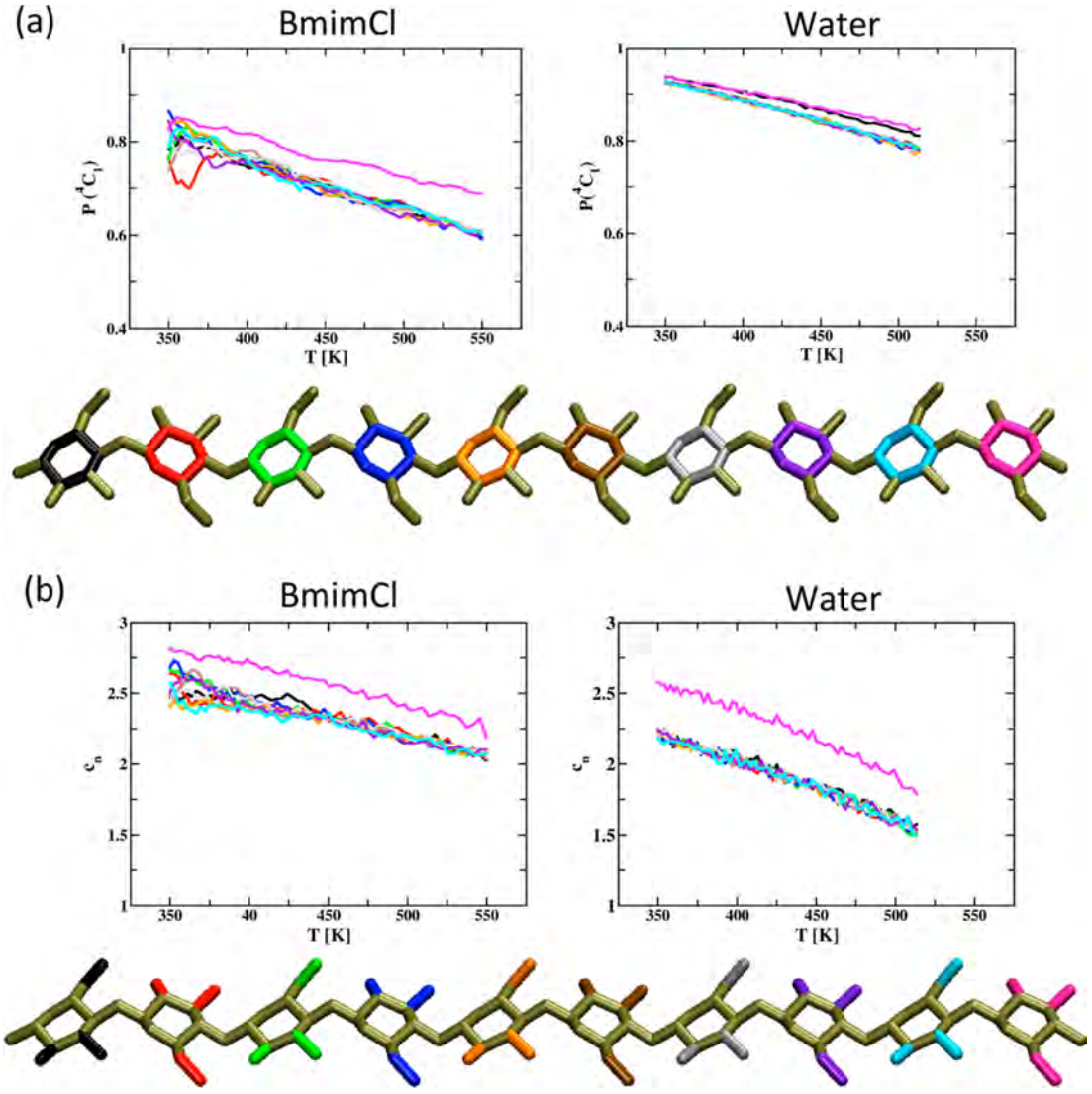

Figure 7. Temperature profiles for (a) the $^4C_1$-chair conformation percentages and (b) the average Cl^- anion or water oxygen coordination numbers c_n around cellulose hydroxyl groups. Colors correspond to the pyanose ring or hydroxyl groups given below the corresponding graph.

identifying distributions of compact and extended cellulose structures.

Another conformational characteristic concerns the pyranose rings, which can adopt several conformations referred to as chair, boat, skew, half-chair, and envelope.[72] While the most stable ring conformation of D-glucopyranose is the $^4C_1$-chair,[73] other conformations are adopted by ring flipping or puckering. We derived the $^4C_1$ population, $P(^4C_1)$, by calculating the angles of the three improper torsions C4−O5−C2−C1, O5−C2−C4−C3, and C2−C4−O5−C5. Following ref 74, the $^4C_1$ conformation is characterized by a value of 35° for these improper torsions (we apply a tolerance value of ±15° in our analysis). The temperature dependence of $P(^4C_1)$ is shown in Figure 7a. The deviation of the pyranose ring conformation from the stable $^4C_1$ is increased at elevated temperatures. Clearly, the ring flipping occurs more often in BmimCl than in water. This is in accord with other results presented in this section supporting the fact that the cellulose chain is more flexible in BmimCl than in water.

The REMD simulations were performed on a decamer as the study of longer cellulose chains would have required larger simulation systems and a much greater number of replicas. However, because cellulose solubility is independent of chain length for DP > 8,[75] the present results derived from simulations of cellulose 10-mers should be applicable to longer chains. Nevertheless, it is useful to determine whether the current results hold for a larger cellulose chain. To this end, we have additionally simulated cellulose 20-mers at three different temperatures around the corresponding pretreatment temperatures in water (T = 350, 375, and 400 K) and in BmimCl (T = 400, 450, and 500 K). On the basis of the time evolution of R_g in these additional simulations shown in Supporting Information, Figure S6, the cellulose 20-mer has much fewer transitions between extended and collapsed conformations, demonstrating the need for an enhanced sampling approach such as REMD. Moreover, while overall structural parameters, such as R_g, are ∼2 times greater for the 20-mer compared to the 10-mer at any of the given temperatures, all the other cellulose conformations analyzed in this study have comparable relative populations as shown in Supporting Information, Table S2. This shows that the local structural properties of cellulose are not dependent on the polymer chain length, and it validates the fact that meaningful conclusions for the cellulose dissolution

dx.doi.org/10.1021/jp502889c | J. Phys. Chem. B 2014, 118, 11037−11049

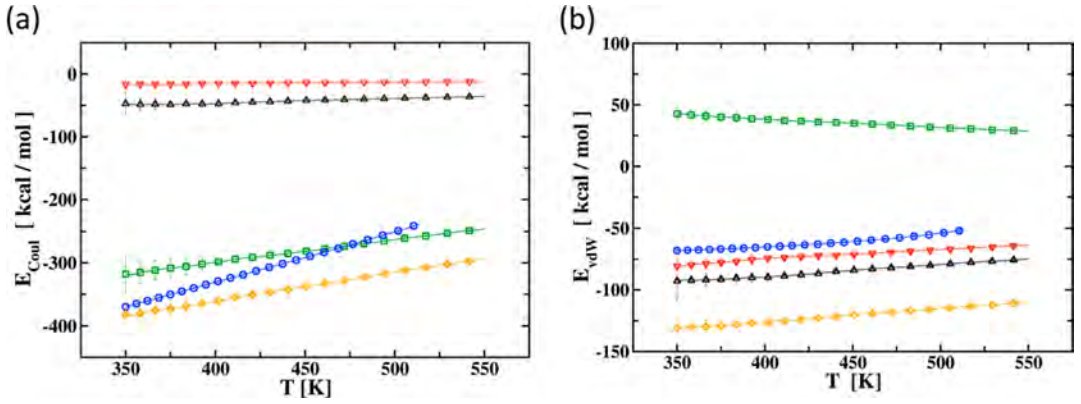

Figure 8. Decomposition of solute−solvent interaction energies into Coulomb (a) and van der Waals (b) contributions. Profiles are given for interactions between the entire cellulose molecule and water (blue circles), BmimCl (orange diamonds), only the Cl^- anion (green squares), only the $Bmim^+$ cation head group (black upward triangles), and only the $Bmim^+$ cation tail group (red downward triangles).

abilities of the two solvents can be drawn from the results based on simulations of a decamer.

3.2. Cellulose−Solvent Interactions. A good cellulose solvent must make favorable interactions with both the polar and the nonpolar parts of the amphiphilic solute. It has been shown that imidazolium-based ILs are capable of breaking hydrogen bonds and separating chains in large cellulose aggregates.[42] It is desirable to know to what extent these interactions take place in the dissolved state of an individual cellulose chain. To this end, we first investigate the binding of Cl^- anions and water molecules to the polar cellulose hydroxyl groups O2H, O3H, and O6H. These sites form hydrogen bonds with water oxygens (average separation of 1.8 Å) or with Cl^- anions (average separation of 2.4 Å). Average coordination numbers derived from site−site pair correlation functions describe the probability of binding. These numbers reveal that the O2H hydroxyl groups are most likely bound (at 350 K, 95% probability for Cl^- and 85% for water oxygen), followed by the O6H (85%, 80%) and the O3H hydroxyls (80%, 55%). Moreover, the probabilities indicate that Cl^- anions bind to these groups stronger than water molecules do, consistent with the notion that the hydrogen bond basicity of the anion determines its dissolution ability. The fact that O3H hydroxyls are the least solvent-coordinated of the three hydroxyl groups is due to the formation of intramolecular O3H′···O5 hydrogen bonds as discussed in the previous section. This suggests that the higher coordination of hydroxyl groups by Cl^- than by water molecules results in greater disruption of the O3H′···O5 hydrogen bonds, thus leading to the cellulose chain being more flexible in BmimCl.

The sum of coordination numbers, c_n, around all hydroxyls of individual glucose units is given in Figure 7b. The binding of solvent to the terminal monomer is strong because of the availability of its O3H hydrogen, which cannot form an intramolecular O3H′···O5 hydrogen bond. The decline of c_n with temperature is consistent with the gain in entropy upon solvent liberation. Interestingly, the water oxygen profile, which has a value of <1.5 at the highest temperature, decreases more sharply than the Cl^- profile. The coordination number of 2−2.5 Cl^- anions per glucose unit agrees well with previous results.[47,76] The higher coordination numbers and the slower decay of the Cl^- profile compared to water show that the anion binds to cellulose more strongly.

Three-dimensional spatial distributions underline the stronger interaction of Cl^- versus water molecules with cellulose (Supporting Information, Figure S8). The anions occupy distinct positions around the hydroxyl groups O2H, O3H, and O6H at densities 5 times higher than that of bulk BmimCl. Density distributions for water oxygens show an average accumulation of water with densities up to 1.8 times its bulk density mainly around the O2H/O3H hydroxyls and around the glucose rings. This analysis confirms the relatively high density of Cl^- around hydroxyls, indicating strong hydroxyl-anion binding, which may contribute to the more effective dissolution of cellulose in BmimCl than in water.

As shown in previous work on cellulose fibers,[43] the cation $Bmim^+$ adopts preferred orientations with respect to proximal surface monomers on cellulose fibers. No specific orientations are observed in the present simulations of a single cellulose chain. Spatial distributions of atoms from the $Bmim^+$ head group show density peaks around the glucose unit at values of 1.5 times the value of bulk BmimCl (Supporting Information, Figure S8). These peaks are located on top of the glucose ring and near the equatorially positioned hydroxyls, but no distinct site−site interactions were found.

Gross et al.[47] have recently reported clearly higher densities of BmimCl ions and water molecules around cellulose chains. In their study, Cl^- anions were found around cellulose hydroxyls with average densities up to 15 times that of bulk BmimCl, and even $Bmim^+$ cations and water molecules were found to accumulate above and below the glucose rings, with average densities of 3.5−4 times that of their bulk values. The reason for their values being significantly higher than those found here is probably that in ref 47 the cellulose chains were simulated with restraints on the terminal residues (and on all residues during equilibration) to keep the chain extended and thus effectively flat during the entire simulation, which lasted only 30 ns. The present REMD simulations, in contrast, were performed on an unrestrained cellulose chain.

To further investigate the interaction between solute and solvent, we decomposed the interaction energies between the solvated cellulose decamer and its solvent molecules into Coulomb (E_{Coul}) and van der Waals (E_{vdW}) contributions. Figure 8 shows that cellulose−BmimCl interactions are more favorable than those of cellulose with water. While all solute−solvent interactions become less favorable with temperature, E_{Coul} for the cellulose−water interaction is the most affected. However, at the optimal cellulose pretreatment temperature, that is, at 375 K in water and at 425−450 K in BmimCl, the

dx.doi.org/10.1021/jp502889c | J. Phys. Chem. B 2014, 118, 11037−11049

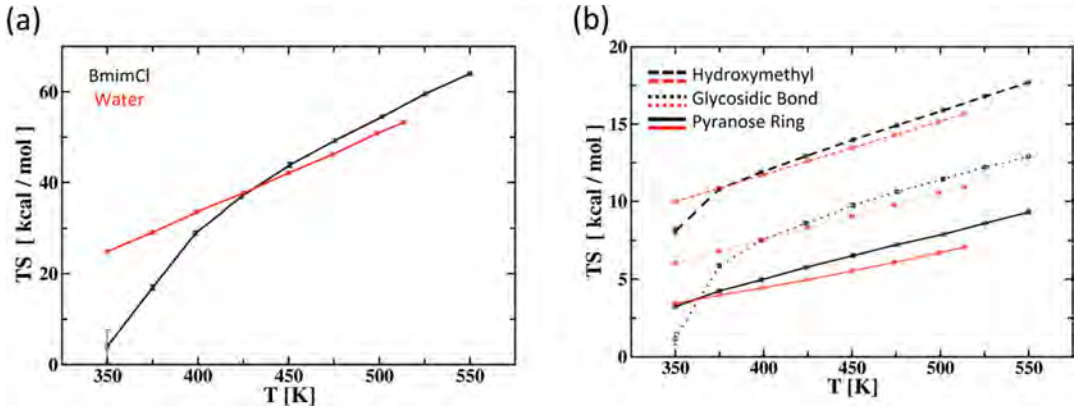

Figure 9. (a) Configurational entropy contribution to the free energy of solvation of cellulose in BmimCl (black) and in water (red) based on all cellulose torsions. (b) Configurational entropy contribution to the free energy of solvation of cellulose in BmimCl (black) and in water (red) based on torsions from the hydroxymethyl group (dashed) or from the glycosidic bond (dotted) or from the pyranose ring (solid) only.

corresponding cellulose−solvent Coulomb interaction energies are similar ($E_{Coul} \approx -350$ kcal/mol).

Consistent with the results on Cl^- coordination of the cellulose hydroxyl groups, E_{Coul} is significantly stronger for cellulose−Cl^- than for cellulose−$Bmim^+$ in the BmimCl solution. However, E_{vdW} is positive for the cellulose−Cl^- interaction but negative for the cellulose−$Bmim^+$ interaction. This corresponds to favorable interaction between cellulose and both the methylimidazole head group and the aliphatic tail group of the cation. In fact, all E_{Coul} and E_{vdW} profiles are comparable for the two $Bmim^+$ moieties.

Additionally, monomer-wise separation of these solute−solvent interaction energies reveals that E_{Coul} lies between −37 and −27 kcal/mol/glucose in BmimCl and between −35 and −22 kcal/mol/glucose in water depending on the temperature (Supporting Information, Figure S9). The terminal monomers have lower electrostatic interaction energies due to the exposure of the additional polar hydroxyl groups at O1H′ and O4H. The corresponding van der Waals interaction energy is about −12 to −10 kcal/mol/glucose in BmimCl and about −7 to −5 kcal/mol/glucose in water.

These findings show that cellulose chain solvation is facilitated by the interplay of both IL components. The larger cation has more favorable van der Waals interactions with cellulose than does water, and the smaller anion has more favorable Coulomb interactions. The presented interaction energies between the cellulose decamer and its solvent environment, taken together with the analysis of distinct interaction sites between solute and solvent molecules, all imply a more favorable enthalpy of single-chain solvation in BmimCl than in water.

3.3. Cellulose Configurational Entropy. To understand the differential dissolution of cellulose in the two solvents, in addition to the enthalpy contribution the difference in entropy has to be addressed. The above results on cellulose conformational distributions have indicated the solute to be more dynamic in the IL than in water. Therefore, it is of interest to estimate the absolute configurational entropy of the chain in the two solvents.

The most widely used analytical method for the calculation of conformational entropies from simulations is the quasi-harmonic (QH) approximation that estimates the absolute entropy of a molecule as the sum of entropy contributions from its degrees of freedom.[64,77−79] The QH method has been applied for the analysis of configurational entropy of various molecular systems, such as peptides, DNA, and hydrocarbons.[80−82] Here, we use this approach mainly as a means of roughly estimating the conformational flexibility of cellulose in the two solvents. It is known that the QH analysis overestimates the entropy value due to artifacts arising from anharmonicity and pairwise correlations,[83,84] and thus correction terms and various alternative approaches have recently been proposed.[85−90] Here, we apply a model that evaluates first-order entropies independently based on their probability distribution and that determines correlations based on the QH method.[91] We use 120 torsional angles along the decamer chain as the relevant degrees of freedom. This approach, combined with enhanced phase-space sampling, is expected to provide robust results on qualitative differences in cellulose conformational flexibility between the two solvents.

Figure 9a shows the temperature profiles for the configurational entropies calculated using all torsional angles of the cellulose chain in BmimCl and in water. Clearly, above ∼425 K the entropy is higher for cellulose in BmimCl than in water, indicating that the solute is more dynamic in the IL than in water at elevated temperatures. Performing the same calculation using only the two glycosidic bond torsions (C4′−O4′−C1−O5 and C5′−C4′−O4′−C1), only those two associated with the hydroxymethyl groups (O5−C5−C6−O6 and C5−C6−O6−H6O), or only two such torsions from the pyranose rings (C5−C4−C3−C2 and C2−C1−O5−C5) allows us to compare the difference in the configurational entropy with respect to these components. This analysis corresponds to diagonalizing a submatrix of the covariance matrix obtained for the entire cellulose chain while neglecting all the off-diagonal block correlations. This corresponds to an approximate decomposition because the sum of the estimated entropy values for the individual components will not add up to the total entropy of the entire chain. Nevertheless, this allows us to make a qualitative assessment of the conformational flexibility of individual cellulose parts in the two solvents. As shown in Figure 9b, the value of the configurational entropy contribution is highest for the hydroxymethyl groups followed by the glycosidic bonds and the pyranose rings in either solvent. This suggests that the hydroxymethyl rotamer is the most flexible part and the pyranose ring structure is the least flexible part of a glucose unit. Interestingly, all three moieties are estimated to be more flexible in BmimCl than in water. Taken together, this

analysis confirms that cellulose is more dynamic in the IL than in water, and that this higher mobility is present in all parts of the glucose unit.

In a previous study, the intramolecular contribution to the entropy change upon cellulose dissolution was found to be more favorable in water than in BmimCl,[92] which seems to be in contrast to our result. However, in ref 92, the authors used a two-phase thermodynamic model, in which the entropy contribution from intramolecular degrees of freedom was derived from the density of states of an ideal solid system based on sub-ns simulations. Thus, the conformational dynamics captured for the entropy calculation take place at a much smaller timescale in the previous work[92] than in the present study, where the intramolecular entropy is estimated from configurational probability distributions derived from 100 ns of REMD.

4. CONCLUSION

In this study, we have examined the structure and dynamics of a fully dissolved cellulose decamer in BmimCl and in water with REMD simulations. We performed 100 ns of REMD between 350 and 550 K, which is necessary for the sampling of a variety of cellulose structures in a solvent such as BmimCl. Although global size-related properties of the decamer are comparable in the two solvents, differences are found in the flexibility and conformations of cellulose. For example, in both solvents the temperature profiles of R_g are similar, but the temperature profiles of $P(\mathrm{GG})/P(\mathrm{GT})$ or $P(\mathrm{O3H'\cdots O5})$ are not. Also, cellulose $\phi-\psi$ scatter plots reveal distinct BmimCl and water basins. Furthermore, higher conformational variability of cellulose in BmimCl is indirectly suggested by a wider free-energy basin for the order parameters $P(\mathrm{GG})/P(\mathrm{GT})$ and $P(\mathrm{O3H'\cdots O5})$ and by a larger variance in their corresponding temperature profiles. The analysis of ring puckering indicates greater flexibility of pyranose rings in BmimCl compared to water. All of the above-mentioned differences in local cellulose structural properties in BmimCl compared to water may lead to the greater dissolution ability of the IL.

A complete understanding of the differential solvation of a cellulose chain in BmimCl and in water will require simulations of the complete fiber-dissolution process, which takes place on timescales significantly larger than presently accessible to atomistic MD. However, the simulations presented here do provide some relevant insight. On the basis of REMD enhanced sampling, the results suggest that the efficient dissolution of cellulose in BmimCl may arise from favorable solute−solvent interactions coupled with an increase in cellulose conformational flexibility. A fundamental knowledge of the driving force for the more efficient cellulose dissolution in ILs than in water will enable us to improve the biomass pretreatment process, which is an essential step in biofuel production.

■ ASSOCIATED CONTENT

Supporting Information

Additional chapters discussing the replica-exchange molecular dynamics and the cellulose polymer structure and additional figures and tables can be found in the Supporting Information. This material is available free of charge via the Internet at http://pubs.acs.org.

■ AUTHOR INFORMATION

Corresponding Author

*E-mail: smithjc@ornl.gov.

Notes

The authors declare no competing financial interest.

■ ACKNOWLEDGMENTS

This research was funded from the BioEnergy Science Center, a DOE Bioenergy Research Center supported by the Office of Biological and Environmental Research in the DOE Office of Science. It was also supported in part by the National Science Foundation through XSEDE resources provided by the National Institute of Computational Sciences under Grant number TG-MCA08X032.

■ REFERENCES

(1) Rogers, R.; Seddon, K. Ionic Liquids—Solvents of the Future? *Science* **2003**, *302*, 792−793.

(2) Plechkova, N.; Seddon, K. Applications of Ionic Liquids in the Chemical Industry. *Chem. Soc. Rev.* **2008**, *37*, 123−150.

(3) Rogers, R. D.; Seddon, K. R. *Ionic Liquids: Industrial Applications for Green Chemistry*; American Chemical Society: Washington, DC, 2002.

(4) Wasserscheid, P.; Welton, T. *Ionic Liquids in Synthesis*; Wiley-VCH: Weinheim, Germany, 2007.

(5) Atkins, M. P.; Davey, P. N.; Fitzwater, G.; Rouher, O.; Seddon, K. R.; Swindall, W. J. *Ionic Liquids: A Map for Industrial Innovation*; Q0001; QUILL: Belfast, Ireland, 2004.

(6) Heintz, A.; Wertz, C. Ionic Liquids: A Most Promising Research Field in Solution Chemistry and Thermodynamics. *Pure Appl. Chem.* **2006**, *78*, 1587−1593.

(7) Chuanfu, L.; Runcang, S.; Zhang, A.; Weiying, L. Dissolution of Cellulose in Ionic Liquids and Its Application for Cellulose Processing and Modification. In *Cellulose Solvents: For Analysis, Shaping and Chemical Modification*; Liebert, T. F., Heinze, T. J., Edgar, K. J., Eds.; American Chemical Society: Washington, DC, **2010**; Vol. *1033*, pp 287−297.

(8) Sun, N.; Rodriguez, H.; Rahman, M.; Rogers, R. Where Are Ionic Liquid Strategies Most Suited in the Pursuit of Chemicals and Energy from Lignocellulosic Biomass? *Chem. Commun.* **2011**, *47*, 1405−1421.

(9) Wang, H.; Gurau, G.; Rogers, R. Ionic Liquid Processing of Cellulose. *Chem. Soc. Rev.* **2012**, *41*, 1519−1537.

(10) Luo, J.; Cai, M.; Gu, T. Pretreatment of Lignocellulosic Biomass Using Green Ionic Liquids. In *Green Biomass Pretreatment for Biofuels Production*; Gu, T., Ed.; Springer: Netherlands, 2013; pp 127−153.

(11) Li, C.; Sun, L.; Simmons, B.; Singh, S. Comparing the Recalcitrance of Eucalyptus, Pine, and Switchgrass Using Ionic Liquid and Dilute Acid Pretreatments. *BioEnergy Research* **2013**, *6*, 14−23.

(12) Dadi, A.; Varanasi, S.; Schall, C. Enhancement of Cellulose Saccharification Kinetics Using an Ionic Liquid Pretreatment Step. *Biotechnol. Bioeng.* **2006**, *95*, 904−910.

(13) Liu, L.; Chen, H. Enzymatic Hydrolysis of Cellulose Materials Treated with Ionic Liquid [Bmim] Cl. *Chin. Sci. Bull.* **2006**, *51*, 2432−2436.

(14) Kim, S.-J.; Dwiatmoko, A.; Choi, J.; Suh, Y.-W.; Suh, D.; Oh, M. Cellulose Pretreatment with 1-*N*-Butyl-3-Methylimidazolium Chloride for Solid Acid-Catalyzed Hydrolysis. *Bioresour. Technol.* **2010**, *101*, 8273−8279.

(15) Li, C.; Knierim, B.; Manisseri, C.; Arora, R.; Scheller, H.; Auer, M.; Vogel, K.; Simmons, B.; Singh, S. Comparison of Dilute Acid and Ionic Liquid Pretreatment of Switchgrass: Biomass Recalcitrance, Delignification and Enzymatic Saccharification. *Bioresour. Technol.* **2010**, *101*, 4900−4906.

(16) Cheng, G.; Varanasi, P.; Li, C.; Liu, H.; Melnichenko, Y.; Simmons, B.; Kent, M.; Singh, S. Transition of Cellulose Crystalline Structure and Surface Morphology of Biomass as a Function of Ionic Liquid Pretreatment and Its Relation to Enzymatic Hydrolysis. *Biomacromolecules* **2011**, *12*, 933−941.

(17) Arora, R.; Manisseri, C.; Li, C.; Ong, M.; Scheller, H.; Vogel, K.; Simmons, B.; Singh, S. Monitoring and Analyzing Process Streams

Towards Understanding Ionic Liquid Pretreatment of Switchgrass (Panicum Virgatum L.). *BioEnergy Research* **2010**, *3*, 134−145.
(18) Himmel, M.; Ding, S.-Y.; Johnson, D.; Adney, W.; Nimlos, M.; Brady, J.; Foust, T. Biomass Recalcitrance: Engineering Plants and Enzymes for Biofuels Production. *Science* **2007**, *315*, 804−807.
(19) Alvira, P.; Tomás-Pejó, E.; Ballesteros, M.; Negro, M. J. Pretreatment Technologies for an Efficient Bioethanol Production Process Based on Enzymatic Hydrolysis: A Review. *Bioresour. Technol.* **2010**, *101*, 4851−4861.
(20) Langan, P.; Gnanakaran, S.; Rector, K.; Pawley, N.; Fox, D.; Cho, D.; Hammel, K. Exploring New Strategies for Cellulosic Biofuels Production. *Energy Environ. Sci.* **2011**, *4*, 3820−3833.
(21) Zhao, B.; Greiner, L.; Leitner, W. Cellulose Solubilities in Carboxylate-Based Ionic Liquids. *RSC Adv.* **2012**, *2*, 2476−2479.
(22) Zhao, Y.; Liu, X.; Wang, J.; Zhang, S. Effects of Cationic Structure on Cellulose Dissolution in Ionic Liquids: A Molecular Dynamics Study. *ChemPhysChem* **2012**, *13*, 3126−3133.
(23) Ohira, K.; Abe, Y.; Kawatsura, M.; Suzuki, K.; Mizuno, M.; Amano, Y.; Itoh, T. Design of Cellulose Dissolving Ionic Liquids Inspired by Nature. *ChemSusChem* **2012**, *5*, 388−391.
(24) Li, C.; Cheng, G.; Balan, V.; Kent, M.; Ong, M.; Chundawat, S.; Sousa, L.; Melnichenko, Y.; Dale, B.; Simmons, B.; Singh, S. Influence of Physico-Chemical Changes on Enzymatic Digestibility of Ionic Liquid and Afex Pretreated Corn Stover. *Bioresour. Technol.* **2011**, *102*, 6928−6936.
(25) Zhang, J.; Zhang, H.; Wu, J.; Zhang, J.; He, J.; Xiang, J. NMR Spectroscopic Studies of Cellobiose Solvation in EmimAc Aimed to Understand the Dissolution Mechanism of Cellulose in Ionic Liquids. *Phys. Chem. Chem. Phys.* **2010**, *12*, 1941−1947.
(26) Bharadwaj, R.; Wong, A.; Knierim, B.; Singh, S.; Holmes, B.; Auer, M.; Simmons, B.; Adams, P.; Singh, A. High-Throughput Enzymatic Hydrolysis of Lignocellulosic Biomass Via In-Situ Regeneration. *Bioresour. Technol.* **2011**, *102*, 1329−1337.
(27) Samayam, I.; Hanson, L.; Langan, P.; Schall, C. Ionic-Liquid Induced Changes in Cellulose Structure Associated with Enhanced Biomass Hydrolysis. *Biomacromolecules* **2011**, *12*, 3091−3098.
(28) Lucas, M.; Wagner, G.; Nishiyama, Y.; Hanson, L.; Samayam, I.; Schall, C.; Langan, P.; Rector, K. Reversible Swelling of the Cell Wall of Poplar Biomass by Ionic Liquid at Room Temperature. *Bioresour. Technol.* **2011**, *102*, 4518−4523.
(29) Çetinkol, Ö.; Dibble, D.; Cheng, G.; Kent, M.; Knierim, B.; Auer, M.; Wemmer, D.; Pelton, J.; Melnichenko, Y.; Ralph, J.; Simmons, B.; Holmes, B. Understanding the Impact of Ionic Liquid Pretreatment on Eucalyptus. *Biofuels* **2010**, *1*, 33−46.
(30) Liu, H.; Sale, K.; Simmons, B.; Singh, S. Molecular Dynamics Study of Polysaccharides in Binary Solvent Mixtures of an Ionic Liquid and Water. *J. Phys. Chem. B* **2011**, *115*, 10251−10258.
(31) Cheng, G.; Varanasi, P.; Arora, R.; Stavila, V.; Simmons, B.; Kent, M.; Singh, S. Impact of Ionic Liquid Pretreatment Conditions on Cellulose Crystalline Structure Using 1-Ethyl-3-Methylimidazolium Acetate. *J. Phys. Chem. B* **2012**, *116*, 10049−10054.
(32) Matthews, J.; Skopec, C.; Mason, P.; Zuccato, P.; Torget, R.; Sugiyama, J.; Himmel, M.; Brady, J. Computer Simulation Studies of Microcrystalline Cellulose Iß. *Carbohydr. Res.* **2006**, *341*, 138−152.
(33) Gross, A.; Chu, J.-W. On the Molecular Origins of Biomass Recalcitrance: The Interaction Network and Solvation Structures of Cellulose Microfibrils. *J. Phys. Chem. B* **2010**, *114*, 13333−13341.
(34) Bergenstråhle, M.; Wohlert, J.; Himmel, M.; Brady, J. Simulation Studies of the Insolubility of Cellulose. *Carbohydr. Res.* **2010**, *345*, 2060−2066.
(35) Beckham, G.; Matthews, J.; Peters, B.; Bomble, Y.; Himmel, M.; Crowley, M. Molecular-Level Origins of Biomass Recalcitrance: Decrystallization Free Energies for Four Common Cellulose Polymorphs. *J. Phys. Chem. B* **2011**, *115*, 4118−4127.
(36) Payne, C.; Himmel, M.; Crowley, M.; Beckham, G. Decrystallization of Oligosaccharides from the Cellulose Iß Surface with Molecular Simulation. *J. Phys. Chem. Lett.* **2011**, *2*, 1546−1550.
(37) Liu, H.; Cheng, G.; Kent, M.; Stavila, V.; Simmons, B.; Sale, K.; Singh, S. Simulations Reveal Conformational Changes of Methylhydroxyl Groups During Dissolution of Cellulose Iß in Ionic Liquid 1-Ethyl-3-Methylimidazolium Acetate. *J. Phys. Chem. B* **2012**, *116*, 8131−8138.
(38) Mostofian, B.; Smith, J. C.; Cheng, X. The Solvation Structures of Cellulose Microfibrils in Ionic Liquids. *Interdiscip. Sci.: Comput. Life Sci.* **2011**, *3*, 308−320.
(39) Zhao, Y.; Liu, X.; Wang, J.; Zhang, S. Effects of Anionic Structure on the Dissolution of Cellulose in Ionic Liquids Revealed by Molecular Simulation. *Carbohydr. Polym.* **2013**, *94*, 723−730.
(40) Liu, H.; Sale, K.; Holmes, B.; Simmons, B.; Singh, S. Understanding the Interactions of Cellulose with Ionic Liquids: A Molecular Dynamics Study. *J. Phys. Chem. B* **2010**, *114*, 4293−4301.
(41) Cho, H.; Gross, A.; Chu, J.-W. Dissecting Force Interactions in Cellulose Deconstruction Reveals the Required Solvent Versatility for Overcoming Biomass Recalcitrance. *J. Am. Chem. Soc.* **2011**, *133*, 14033−14041.
(42) Rabideau, B.; Agarwal, A.; Ismail, A. Observed Mechanism for the Breakup of Small Bundles of Cellulose Iα and Iß in Ionic Liquids from Molecular Dynamics Simulations. *J. Phys. Chem. B* **2013**, *117*, 3469−3479.
(43) Mostofian, B.; Smith, J. C.; Cheng, X. Simulation of a Cellulose Fiber in Ionic Liquid Suggests a Synergistic Approach to Dissolution. *Cellulose* **2013**, *21*, 983−997.
(44) Lindman, B.; Karlström, G.; Stigsson, L. On the Mechanism of Dissolution of Cellulose. *J. Mol. Liq.* **2010**, *156*, 76−81.
(45) Medronho, B.; Romano, A.; Miguel, M.; Stigsson, L.; Lindman, B. Rationalizing Cellulose (in)Solubility: Reviewing Basic Physicochemical Aspects and Role of Hydrophobic Interactions. *Cellulose* **2012**, *19*, 581−587.
(46) Heinze, T.; Schwikal, K.; Barthel, S. Ionic Liquids as Reaction Medium in Cellulose Functionalization. *Macromol. Biosci.* **2005**, *5*, 520−525.
(47) Gross, A.; Bell, A.; Chu, J.-W. Thermodynamics of Cellulose Solvation in Water and the Ionic Liquid 1-Butyl-3-Methylimidazolim Chloride. *J. Phys. Chem. B* **2011**, *115*, 13433−13440.
(48) Nymeyer, H.; Woolf, T.; Garcia, A. Folding Is Not Required for Bilayer Insertion: Replica Exchange Simulations of an Alpha-Helical Peptide with an Explicit Lipid Bilayer. *Proteins* **2005**, *59*, 783−790.
(49) Lu, Z.; Hu, H.; Yang, W.; Marszalek, P. Simulating Force-Induced Conformational Transitions in Polysaccharides with the SMD Replica Exchange Method. *Biophys. J.* **2006**, *91*.
(50) Kannan, S.; Zacharias, M. Simulation of DNA Double-Strand Dissociation and Formation During Replica-Exchange Molecular Dynamics Simulations. *Phys. Chem. Chem. Phys.* **2009**, *11*, 10589−10595.
(51) Han, M.; Hansmann, U. Replica Exchange Molecular Dynamics of the Thermodynamics of Fibril Growth of Alzheimer's Aß-42 Peptide. *J. Chem. Phys.* **2011**, *135*, 065101.
(52) Kirschner, K.; Yongye, A.; Tschampel, S.; González-Outeiriño, J.; Daniels, C.; Foley, L.; Woods, R. Glycam06: A Generalizable Biomolecular Force Field. Carbohydrates. *J. Comput. Chem.* **2008**, *29*, 622−655.
(53) Jorgensen, W.; Chandrasekhar, J.; Madura, J.; Impey, R.; Klein, M. Comparison of Simple Potential Functions for Simulating Liquid Water. *J. Chem. Phys.* **1983**, *79*, 926−935.
(54) Liu, Z.; Huang, S.; Wang, W. A Refined Force Field for Molecular Simulation of Imidazolium-Based Ionic Liquids. *J. Phys. Chem. B* **2004**, *108*, 12978−12989.
(55) Gaussian Version 09 . Frisch, M. J. et al. Gaussian, Inc.: Wallingford, CT, 2009.
(56) Bussi, G.; Donadio, D.; Parrinello, M. Canonical Sampling through Velocity Rescaling. *J. Chem. Phys.* **2007**, *126*, 014101.
(57) Berendsen, H. J. C.; Postma, J. P. M.; Van Gunsteren, W. F.; Dinola, A.; Haak, J. R. Molecular Dynamics with Coupling to an External Bath. *J. Chem. Phys.* **1984**, *81*, 3684−3690.
(58) Gu, Z.; Brennecke, J. Volume Expansivities and Isothermal Compressibilities of Imidazolium and Pyridinium-Based Ionic Liquids. *J. Chem. Eng. Data* **2002**, *47*, 339−345.

(59) Darden, T.; York, D.; Pedersen, L. Particle Mesh Ewald: An N*Log(N) Method for Ewald Sums in Large Systems. *J. Chem. Phys.* **1993**, *98*, 10089−10092.
(60) Essmann, U.; Perera, L.; Berkowitz, M.; Darden, T.; Lee, H.; Pedersen, L. A Smooth Particle Mesh Ewald Method. *J. Chem. Phys.* **1995**, *103*, 8577−8593.
(61) Hess, B.; Bekker, H.; Berendsen, H.; Fraaije, J. Lincs: A Linear Constraint Solver for Molecular Simulations. *J. Comput. Chem.* **1997**, *18*, 1463−1472.
(62) Hess, B.; Kutzner, C.; Van Der Spoel, D.; Lindahl, E. Gromacs 4: Algorithms for Highly Efficient, Load-Balanced, and Scalable Molecular Simulation. *J. Chem. Theory Comput.* **2008**, *4*, 435−447.
(63) Okabe, T.; Kawata, M.; Okamoto, Y.; Mikami, M. Replica-Exchange Monte Carlo Method for the Isobaric−Isothermal Ensemble. *Chem. Phys. Lett.* **2001**, *335*, 435−439.
(64) Karplus, M.; Kushick, J. N. Method for Estimating the Configurational Entropy of Macromolecules. *Macromolecules* **1981**, *14*, 325−332.
(65) Baron, R.; Hünenberger, P. H.; Mccammon, J. A. Absolute Single-Molecule Entropies from Quasi-Harmonic Analysis of Microsecond Molecular Dynamics: Correction Terms and Convergence Properties. *J. Chem. Theory Comput.* **2009**, *5*, 3150−3160.
(66) Di Nola, A.; Berendsen, H. J. C.; Edholm, O. Free Energy Determination of Polypeptide Conformations Generated by Molecular Dynamics. *Macromolecules* **1984**, *17*, 2044−2050.
(67) Tracy, M. A.; Pecora, R. Dynamics of Rigid and Semirigid Rodlike Polymers. *Annu. Rev. Phys. Chem.* **1992**, *43*, 525−557.
(68) Kroon-Batenburg, L. M. J.; Kruiskamp, P. H.; Vliegenthart, J. F. G.; Kroon, J. Estimation of the Persistence Length of Polymers by MD Simulations on Small Fragments in Solution. Application to Cellulose. *J. Phys. Chem. B* **1997**, *101*, 8454−8459.
(69) Saalwächter, K.; Burchard, W.; Klüfers, P. Cellulose Solutions in Water Containing Metal Complexes. *Macromolecules* **2000**, *33*, 4094−4107.
(70) Shen, T.; Langan, P.; French, A. D.; Johnson, G. P.; Gnanakaran, S. Conformational Flexibility of Soluble Cellulose Oligomers: Chain Length and Temperature Dependence. *J. Am. Chem. Soc.* **2009**, *131*, 14786−14794.
(71) Nishiyama, Y.; Langan, P.; Chanzy, H. Crystal Structure and Hydrogen-Bonding System in Cellulose Iβ from Synchrotron X-Ray and Neutron Fiber Diffraction. *J. Am. Chem. Soc.* **2002**, *124*, 9074−9082.
(72) Stoddart, J. F. *Stereochemistry of Carbohydrates*; Wiley: New York, NY, 1971.
(73) Ionescu, A. R.; Bérces, A.; Zgierski, M. Z.; Whitfield, D. M.; Nukada, T. Conformational Pathways of Saturated Six-Membered Rings. A Static and Dynamical Denisty Functional Study. *J. Phys. Chem. A* **2005**, *109*, 8096−8105.
(74) Rao, V. S. R.; Qasba, P. K.; Balaji, P. V.; Chandrasekaran, R. *Conformation of Carbohydrates*; OPA: Amsterdam, The Netherlands, 1998.
(75) Glasser, W. G.; Atalla, R. H.; Blackwell, J.; Malcolm Brown, R., Jr.; Burchard, W.; French, A. D.; Klemm, D. O.; Nishiyama, Y. About the Structure of Cellulose: Debating the Lindman Hypothesis. *Cellulose* **2012**, *19*, 589−598.
(76) Youngs, T. G. A.; Hardacre, C.; Holbrey, J. D. Glucose Solvation by the Ionic Liquid 1,3-Dimethylimidazolium Chloride: A Simulation Study. *J. Phys. Chem. B* **2007**, *111*, 13765−13774.
(77) Levy, R. M.; Karplus, M.; Kushick, J. N.; Perahia, D. Evaluation of the Configurational Entropy for Proteins: Applications to Molecular Dynamics Simulations of an A-Helix. *Macromolecules* **1984**, *17*, 1370−1374.
(78) Andricoaei, I.; Karplus, M. On the Calculation of Entropy from Covariance Matrices of the Atomic Fluctuations. *J. Chem. Phys.* **2001**, *115*, 6289−6292.
(79) Schlitter, J. Estimation of Absolute and Relative Entropies of Macromolecules Using the Covariance Matrix. *Chem. Phys. Lett.* **1993**, *215*, 617−621.
(80) Baron, R.; De Vries, A. H.; Hünenberger, P. H.; Van Gunsteren, W. F. Comparison of Atomic-Level and Coarse-Grained Models for Liquid Hydrocarbons from Molecular Dynamics Configurational Entropy Estimates. *J. Phys. Chem. B* **2006**, *110*, 8464−8473.
(81) Dolenc, J.; Baron, R.; Oostenbrink, C.; Koller, J.; Van Gunsteren, W. F. Configurational Entropy Change of Netropsin and Distamycin Upon DNA Minor-Groove Binding. *Biophys. J.* **2006**, *91*, 1460−1470.
(82) Missimer, J. H.; Steinmetz, M. O.; Baron, R.; Winkler, F. K.; Kammerer, R. A.; Daura, X.; Van Gunsteren, W. F. Configurational Entropy Elucidates the Role of Salt-Bridge Networks in Protein Thermostability. *Protein Sci.* **2007**, *16*, 1349−1359.
(83) Chang, C.-E.; Chen, W.; Gilson, M. K. Evaluating the Accuracy of the Quasiharmonic Approximation. *J. Chem. Theory Comput.* **2005**, *1*, 1017−1028.
(84) Baron, R.; Van Gunsteren, W. F.; Hünenberger, P. H. Estimating the Configurational Entropy from Molecular Dynamics Simulations: Anharmonicity and Correlation Corrections to the Quasi-Harmonic Approximation. *Trends Phys. Chem.* **2006**, *11*, 87−122.
(85) Rojas, O. L.; Levy, R. M.; Szabo, A. Corrections to the Quasiharmonic Approximation for Evaluating Molecular Entropies. *J. Chem. Phys.* **1986**, *85*, 1037−1043.
(86) Hnizdo, V.; Darian, E.; Fedorowicz, A.; Demchuk, E.; Li, S.; Singh, H. Nearest-Neighbor Nonparametric Method for Estimating the Configurational Entropy of Complex Molecules. *J. Comput. Chem.* **2007**, *28*, 655−668.
(87) Li, D.-W.; Khanlarzadeh, M.; Wang, J.; Huo, S.; Brüschweiler, R. Evaluation of Configurational Entropy Methods from Peptide Folding−Unfolding Simulation. *J. Phys. Chem. B* **2007**, *111*, 13807−13813.
(88) Killian, B. J.; Yudenfreund Kravitz, J.; Gilson, M. K. Extraction of Configurational Entropy from Molecular Simulations Via an Expansion Approximation. *J. Chem. Phys.* **2007**, *127*, 024107.
(89) Nguyen, P. H.; Derreumaux, P. Configurational Entropy: An Improvement of the Quasiharmonic Approximation Using Configurational Temperature. *Phys. Chem. Chem. Phys.* **2012**, *14*, 877−886.
(90) Numata, J.; Knapp, E.-W. Balanced and Bias-Corrected Computation of Conformational Entropy Differences for Molecular Trajectories. *J. Chem. Theory Comput.* **2012**, *8*, 1235−1245.
(91) Harpole, K. W.; Sharp, K. A. Calculation of Configurational Entropy with a Boltzmann-Quasiharmonic Model: The Origin of High-Affinity Protein-Ligand Binding. *J. Phys. Chem. B* **2011**, *115*, 9461−9472.
(92) Gross, A. S.; Bell, A. T.; Chu, J.-W. Entropy of Cellulose Dissolution in Water and in the Ionic Liquid 1-Butyl-3-Methylimidazolium Chloride. *Phys. Chem. Chem. Phys.* **2012**, *14*, 8425−8430.